SAND2018-3581R

Sandia National Laboratories
Operated for the U.S. Department of Energy
National Technology & Engineering Solutions of Sandia
Albuquerque, New Mexico 87185-0834

date: 4 April 2018

to: Open Distribution (Unclassified, Unlimited Release)

from: Allen Roach, Department 2241

subject: Laser Spot Welding using an ALE Finite Element Method

This memo consists of a manuscript draft that was never published, but was prepared in 2002 at Sandia. It is used as a user-guide for running simulations of laser welding with Sandia's Goma 6.0 software.

1

[1] Sandia National Laboratories is a multimission laboratory managed and operated by National Technology & Engineering Solutions of Sandia, LLC, a wholly owned subsidiary of Honeywell International Inc., for the U.S. Department of Energy's National Nuclear Security Administration under contract DE-NA0003525.

Laser Spot Weld Modeling using an ALE Finite Element Method

M. P. Kanouff[1], A. Kassinos[2], D. R. Noble and P. R. Schunk[3]

Sandia National Laboratories, Livermore, CA 94550[1], and Albuquerque, NM 87185[3]

CTC/United Defense, Santa Clara, CA 95050[2]

Calculations of the formation of an axisymmetric keyhole in a laser heated weld pool were carried out using an arbitrary Lagrangian/Eulerian finite element method. A one dimensional gas dynamics model is used to provide the recoil pressure caused by rapid heating and evaporation from the high temperature molten surface. The vapor recoil pressure is then used as a boundary condition to calculate the deformation of the free surface and the resulting fluid motion in the molten zone. A moving finite element mesh is used to track the time dependent and a priori unknown shapes of the solid and liquid phase regions. The results show that, depending on the laser power, the shape of the free surface follows closely that of the solid/liquid phase boundary with a thin layer of liquid between these two boundaries.

Nomenclature

c_p	specific heat
F_{k0}	view factor from keyhole to keyhole opening
H_{fg}	heat of evaporation
H_{sf}	heat of fusion
k	thermal conductivity
n	coordinate locally normal to interface
p	pressure
p_r	vapor recoil pressure
q_c	convection energy flux
q_e	evaporation energy flux
q_l	laser energy flux
Q	laser power
r	radial coordinate
r_q	radius of laser Gaussian heat flux
R	gas constant
t	time
T	temperature
T_b	boiling temperature at atmospheric pressure
T_m	melting temperature
ΔT_b	temperature difference, T_b-T_m
ΔT_m	temperature difference, T_m-T_∞
u	velocity vector
V_c	velocity scale, $\alpha_0 Q/(r_q^2 \rho c_p \Delta T_m)$
z	axial coordinate

Greek symbols

α effective absorptivity of the keyhole
α_0 absorptivity of a flat surface
β thermal expansion coefficient
γ ratio of specific heats
μ viscosity
θ non-dimensional temperature, $(T-T_\infty)/(T_m-T_\infty)$
ρ density
σ surface tension

Subscripts
k outside of Knudsen layer
L liquid surface
s behind shock wave
sat saturation
v vapor
∞ ambient

Keywords:
Laser Welding, keyhole, vapor recoil, Knudsen layer, weld pool model, thermal-only solution, moving-mesh solution, weld pool shape

Introduction

Lasers provide an excellent heat source for performing welding operations due to the large heat flux that can be obtained. The heat is deposited quickly such that it remains close to the deposition region and only a relatively small amount of energy is required to form a molten pool. This minimizes the size of the heat affected zone (HAZ) that develops in the solid material adjacent to the weld pool. Detrimental phase changes driven by large temperatures can occur in this zone. These high temperatures also result in a large thermal expansion of the zone that is partially constrained by the relatively cool material that surrounds it. This results in plastic deformation, the development of residual stresses upon cooling, and overall part distortion. The small amount of energy used in the laser welding process helps to reduce the residual stresses and distortion.

In the laser welding process the laser beam is directed to a metal surface which melts material forming a small molten pool. The liquid metal is heated to high temperatures resulting in large evaporation rates. The rapid evaporation creates a large recoil pressure on the surface of the molten layer depressing it downward. The weld pool then takes the structure of a vertical vapor core, called a keyhole, surrounded by molten metal. Large values of the laser power can result in recoil pressures that cause material to be ejected from the weld pool. This is very undesirable because it leaves a hole or crater at the top of the solidified weld and may result in a loss of seal and a weak weld, in general.

There are two different modes of operation for laser welding, continuous and pulsed. In both modes the laser travels relative to the work piece along the seam to be joined. In the continuous-mode, the laser is kept on continuously while in the pulsed-mode the laser is pulsed such that a series of overlapping spot welds are made along the joint seam. The two modes of operation are fundamentally

different in that a steady three dimensional traveling weld pool can develop in the continuous-mode, while in the pulsed mode a weld pool is formed and solidified with each pulse. The weld pool in this latter mode is at all times unsteady but simpler to analyze because it may be approximated as axi-symmetric.

We consider here the transient development of a single axisymmetric weld pool, corresponding to what may occur during one pulse of the pulsed mode of operation of the laser welding process. An arbitrary Lagrangian/Eulerian finite element model is used to calculate the momentum and energy transport in the pool and surrounding solid. There are no simplifying assumptions used for the shape of the free surface of the pool, rather it is calculated based on the distributions for the vapor recoil pressure and hydrodynamic forces and the surface tension.

Background

A number of investigators have developed models predicting the shape of a keyhole in a laser heated molten pool. Lambrakos, et al. [1] reported some of the earlier calculations of keyhole shapes in laser welding. They calculated the three dimensional shapes of a traveling keyhole and weld pool. The calculations were simplified by assuming that the vapor-liquid interface (i.e. free surface) was defined by the location where the temperature was equal to the boiling temperature. Kroos, et al. [2] developed a simplified model for a traveling keyhole that was assumed to have a cylindrical shape. The temperature of the keyhole surface was calculated based on an energy balance between the incident laser energy flux, the heat conduction into the surrounding liquid, and the energy flux lost by evaporation, where simplified estimates were used for each. The keyhole surface energy balance was coupled with an evaporation model that accounted for non-equilibrium between vapor and liquid phases. The evaporation model provided a vapor recoil force which was balanced with the surface tension force (acting to close the keyhole) to determine the radius of the keyhole. Ganesh, et al. [3] modeled the laser drilling process, which is similar to laser welding in that a keyhole forms within the molten zone. They used an axisymmetric finite-volume model with the volume-of-fluid method to calculate the shape of the free surface of the keyhole.

Many investigators assume that the laser energy is absorbed at the surface of the condensed phase and neglect absorption by the vapor phase. These assumptions are based upon estimates that show the vapor temperature and its absorptivity are small [4,5]. Some researchers, however, argue that the vapor in the keyhole may be heated to high enough temperatures to ionize and become a plasma such that it absorbs a significant amount of the laser energy. Solana and Ocana [6] considered the case of direct absorption of the laser energy by this plasma in a traveling keyhole and weld pool. A temperature dependent absorptivity was used for the plasma. They assumed that conduction was the only mode of heat transfer in all phases, and that the laser energy absorbed by the plasma acted like a volumetric heat source. The portion of the laser energy not absorbed by the plasma was applied as a heat flux on the surface of the keyhole. A balance between the evaporation recoil force and surface tension force was used to determine the shape of the keyhole.

A more detailed analysis of the local dynamics of the keyhole was carried out by Matsunawa, et al.

[7], who developed a model for the forward portion of a traveling keyhole. They used a local energy balance between the incident energy, conduction into the liquid and the evaporation loss, along with a local momentum balance between the evaporative recoil force, surface tension and fluid inertia. Their results showed that humps develop on the keyhole surface such that the incident laser energy varied spatially between large and small values depending on the surface normal component of the laser energy flux vector. This resulted in a local keyhole wall position that was never in a steady state, i.e. the recoil force dominated the surface tension force in large laser energy flux regions while the reverse was true in small laser energy flux regions. As a result the humps on the keyhole surface continually moved down toward the bottom of the keyhole.

When a laser beam strikes a surface some of the energy is reflected. If the laser is directed into a deep keyhole then multiple reflections take place and a significant difference can develop between the incident laser energy distribution and the absorbed energy distribution. This problem was considered by Wang and Wei [8], who calculated the diffuse and specular reflections of laser energy within the a keyhole with a prescribed shape. Their results showed that the absorbed laser energy distribution can be described in terms of two regions; 1) the lower portion of the keyhole where primarily direct incident and diffusely reflected laser energy is absorbed, and 2) the upper portion of the keyhole where primarily direct incident and specularly reflected laser energy is absorbed. An overall effective absorptivity of the keyhole was calculated based on these results that was shown to increase with keyhole depth.

Many of the keyhole formation calculations that have been reported in the literature used an evaporation model whose origin can be traced to Anisimov [9] and Knight [10]. Anisimov considered the vaporization of a laser heated metal into a vacuum. He assumed the vapor to be a non-absorbing ideal gas and the metal surface temperature to be constant. Due to the large difference between the equilibrium vapor state corresponding to the temperature of the metal surface and the actual vapor state that develops near the surface when the evaporation occurs in a vacuum, a thin ‘Knudsen’ layer will exist adjacent to the surface where there is a large departure from thermodynamic equilibrium. Anisimov treated this Knudsen layer like a discontinuity and used the method of moments from kinetic theory to derive relationships between the surface temperature and the temperature, density and velocity of the gas outside of the Knudsen layer. These relationships were solved along with the gas dynamic equations governing the one-dimensional expansion and flow of the vapor away from the surface to obtain the net evaporation rate and recoil pressure. For the case of evaporation into a vacuum the gas flow field takes the structure of a centered rarefaction fan starting downstream of the Knudsen layer.

Knight [10] extended the work of Anisimov by considering the case of evaporation into a background gas with a non-zero initial pressure. In this case the centered rarefaction fan may not occur depending on the evaporation rate and ambient pressure. Also, in this case a shock wave is generated at the surface when evaporation begins, which propagates into the stagnant ambient gas, compressing it and setting it in motion away from the surface.

Evaporation Model

Keyhole formation is driven by the vapor recoil pressure exerted on the surface of the weld pool. This recoil pressure results from the rapid evaporation from the surface that has been heated to high temperatures. We follow the work of Knight [10] for these calculations, which give the boundary conditions used for the keyhole formation calculations. One limitation of this evaporation model is that it neglects all diffusion processes, which means that evaporation does not begin until the surface temperature exceeds the boiling temperature, T_b.

It is assumed that the evaporation rate is steady, the vapor expansion and gasdynamic flow of the vapor and ambient gas are one-dimensional in the direction locally normal to the liquid surface and that the ambient air is a semi-infinite medium. The structure of the flow field is then as shown in Figure 1. The liquid surface is at a constant temperature, T_L, the undisturbed (zero velocity) ambient air has a known pressure, p_∞, and temperature, T_∞. There is a Knudsen layer adjacent to the liquid surface where the vapor escaping from the liquid surface is in a state of thermodynamic non-equilibrium, i.e. the vapor molecules do not have a Maxwellian velocity distribution. This occurs when the equilibrium vapor pressure (i.e. the saturation pressure) corresponding to the surface temperature is large compared to the ambient partial pressure of the vapor. Under these conditions the vapor adjacent to the surface is dominated by recently evaporated material that has not yet experienced the molecular collisions necessary to establish a Maxwellian velocity distribution. The Knudsen layer is estimated to be a few molecular mean free paths thick in order to allow for the molecular collisions to occur that bring the molecules into a state of translational equilibrium at the outer edge of the Knudsen layer.

Knight included the possibility that outside of the Knudsen layer a rarefaction (expansion) fan may form. However, for atmospheric ambient pressure this expansion fan would only occur for very large evaporation rates. Our calculations permit the formation of this fan (i.e. it occurs when the velocity outside of the Knudsen layer becomes sonic) but it was never found to form for the conditions considered in this work.

Outside of the Knudsen layer is a region of vapor with constant and uniform temperature, density and velocity. Next to this region of vapor is a region of air that is also at a constant and uniform temperature, density and velocity. These regions of vapor and air are separated by a line of discontinuity, called a contact discontinuity, where the diffusion processes that would result in the mixing of the two gases are neglected in this analysis. The temperature and density of the gases are discontinuous across the line separating the vapor and air, while the velocity and pressure are equal in these two regions.

A shock wave, which is moving away from the liquid surface with a supersonic velocity relative to the ambient air, separates the moving air from the stagnant ambient air. It is this shock wave which sets the air in motion, and compresses it resulting in an elevated pressure and temperature in this

region relative to the ambient conditions.

A kinetic theory approach is required for the Knudsen layer. The analysis proceeds by constructing an approximate molecular velocity distribution adjacent to the liquid surface. Equations describing the conservation of mass, momentum and energy across the Knudsen layer are developed in terms of this velocity distribution. This gives equations (1) and (2) for the gas temperature, T_k, and density, ρ_k, outside of the Knudsen layer as functions of the liquid surface temperature and the corresponding saturation density, ρ_{sat} [10].

$$\frac{T_k}{T_L} = \left[\sqrt{1+\pi\left(\frac{\gamma-1}{\gamma+1}\frac{m}{2}\right)^2} - \sqrt{\pi}\frac{\gamma-1}{\gamma+1}\frac{m}{2}\right]^2 \tag{1}$$

$$\frac{\rho_k}{\rho_{sat}} = \sqrt{\frac{T_L}{T_k}}\left[\left(m^2+\frac{1}{2}\right)e^{m^2}erfc(m) - \frac{m}{\sqrt{\pi}}\right] + \frac{1}{2}\frac{T_L}{T_k}\left[1-\sqrt{\pi}me^{m^2}erfc(m)\right] \tag{2}$$

Here the quantity, *m*, is closely related to the Mach number at the outer edge of the Knudsen layer, M_k, and is defined as, $m = u_k/(\sqrt{2R_vT_k}) = M_k\sqrt{2/\gamma_v}$, where γ_v and R_v are the ratio of specific heats and the gas constant for the vapor, respectively. The value of m depends on the gas dynamics of the vapor flow away from the surface.

The gas temperature, pressure and density throughout the vapor region (outside of the Knudsen layer) are uniform. The contact discontinuity; that is, the boundary between vapor and air, is an idealization that results due to the neglect of mass diffusion and heat conduction. The velocity and pressure are equal in these regions, $u_k=u_s$ and $p_k=p_s$, where the subscript, s, denotes properties behind the shock wave. Note that, in general, $T_k \neq T_s$ and $\rho_k \neq \rho_s$.

The thermodynamic state and velocity of the air on each side of the shock wave are related by the Rankine-Hugoniot relations, where the most convenient forms for this application are given by Equations (3) and (4). M_k is the Mach number in the vapor, $M_k = u_k/(\sqrt{\gamma_v R_v T_k})$.

$$\frac{p_s}{p_\infty} = 1+\gamma M_k\sqrt{\frac{\gamma_v R_v T_k}{\gamma_\infty R_\infty T_\infty}}\left[\frac{\gamma_\infty+1}{4}M_k\sqrt{\frac{\gamma_v R_v T_k}{\gamma_\infty R_\infty T_\infty}} + \sqrt{1+\left(\frac{\gamma_\infty+1}{4}M_k\sqrt{\frac{\gamma_v R_v T_k}{\gamma_\infty R_\infty T_\infty}}\right)^2}\right] \tag{3}$$

$$\frac{T_s}{T_\infty} = \frac{p_s}{p_\infty}\left(1+\frac{\gamma+1}{\gamma-1}\frac{p_s}{p_\infty}\right)\Big/\left(\frac{p_s}{p_\infty}+\frac{\gamma+1}{\gamma-1}\right) \tag{4}$$

The saturation pressure, p_{sat}, is obtained from equation (5) [11], where p_{sat} is in units of Pa, T_L is in Kelvin, log is base 10, and A, B and C are constants which depend on the material and for iron they

are equal to 19710, 1.27 and 15.33, respectively. This is used to obtain the saturation density, $\rho_{sat}= p_{sat}/(R_v T_L)$, assuming an ideal gas (all gases are assumed to be ideal in this analysis).

$$\log P_{sat} = -\frac{A}{T_L} - B\log T_L + C \tag{5}$$

Equations 1-5 are solved as a function of T_L using an iterative solution method. The vapor was assumed to be iron in the form of a monatomic gas with molecular weight of 56, and γ_v=1.67. The ambient gas was assumed to be air with conditions of p_∞= 1 atm and T_∞ = 295 K. Quantities of particular interest are the recoil pressure, p_r, and rate of energy loss due to evaporation, q_e, given by equations (6a,b).

$$p_r = p_k + \rho_k u_k^2 \quad , \qquad q_e = H_{fg}\rho_k u_k \tag{6a,b}$$

Figure 2 shows results for the saturation vapor pressure, p_{sat}, the recoil pressure, p_r, and the static pressure at the outer edge of the Knudsen layer, p_k. The recoil pressure is much less than the saturation pressure. The shock wave results in values for $p_s= p_k$ which are well above 1 atm (10133 Pa). The recoil pressure is larger than p_k where the difference is the momentum flux of the vapor (Eqn. 6a,b). The expansion fan does not occur until T_L= 5115 K. Figure 2 also shows the rate of energy loss from the liquid surface due to evaporation, q_e. The Mach number, M_k (not shown), increases with T_L, and is 0.37 at T_L = 4000 K. The results for p_r and q_e shown in Figure 2 are used as boundary conditions on the free surface in the weld pool model where they are applied as a function of the local surface temperature.

Mathematical Model of the Weld Pool

The governing equations for mass, momentum and energy conservation are made dimensionless by using the following scales; the width of the laser heat flux distribution, r_q for distance, V_c for velocity, r_q/V_c for time, σ/r_q for pressure, and $\theta = (T-T_\infty)/\Delta T_m$, $\Delta T_m = T_m - T_\infty$, for temperature. The velocity scale, V_c, is derived assuming that the fluid velocity will be of the same order as the velocity of the melt front. It is derived from the energy boundary condition at the melt front (see Eqn. 14) assuming that the energy flux into the front is that of the absorbed laser irradiance. For the purposes of deriving the velocity scale, the heat conducted away from the front into the solid phase is approximated with an idealized solution (see the appendix). The result for the velocity scale is $V_c=\alpha_0 Q/(r_q^2 \rho c_p \Delta T_m)$, where Q is the laser power. The results presented later in this paper show that this scale provides values close to the velocities computed for the free surface, melt front and fluid. Equations (7)-(9) describe, in dimensionless form, mass, momentum and energy conservation.

$$\nabla \bullet u = 0 \tag{7}$$

$$\frac{\partial \boldsymbol{u}}{\partial t} + \boldsymbol{u} \bullet \nabla \boldsymbol{u} = -\frac{1}{W_e}\nabla p + \frac{1}{R_e}\nabla^2 \boldsymbol{u} - \frac{\beta \Delta T_b}{Fr}\frac{\Delta T_m}{\Delta T_b}(\theta - 1) \tag{8}$$

$$\frac{\partial \theta}{\partial t} + \boldsymbol{u} \bullet \nabla \theta = \frac{1}{P_e}\nabla^2 \theta \tag{9}$$

The momentum equation contains three dimensionless parameters, the Weber number, $We=\rho r_q V_c^2/\sigma$, the Reynolds number, $Re=\rho V_c r_q/\mu$, and the dimensionless group, $\beta\Delta T_b/Fr$ ($\Delta T_b = T_b - T_m$), where the Froude number is, $Fr=V_c^2/(r_q\sigma)$. The energy equation contains the Peclet number, $Pe=\rho c_p V_c r_q/k$.

The boundary condition on the free surface for the momentum equation is given by Equation (10), which states that the normal stress in the molten metal, composed of the sum of the pressure and the viscous stress, is balanced by the surface tension acting on the curved surface (2H is the mean curvature, $R_1^{-1} + R_2^{-1}$, where R_1 and R_2 are two orthogonal radii of curvature, or equivalently, 2H may be expressed in terms of an equation for the surface [12]) plus the recoil pressure due to evaporation. Note that the ratio We/Re is equal to the capillary number, $Ca=\mu V_c/\sigma$. A second boundary condition applied at the free surface is that there is zero shear stress. The zero slip condition is applied at the melt front.

$$p + 2C_a\frac{\partial u_n}{\partial n} = 2H + p_r \tag{10}$$

The boundary condition on the free surface for the energy equation is given by Equation (11), which states that the net heat flux into the molten metal is given by the dot product of the laser heat flux vector with the local surface normal, minus the energy lost by evaporation and convection. This energy boundary condition is actually applied over the entire top surface including the solid domain. The convection loss is given by $q_c = h\,(T - T_\infty)$, where $h = 1000\ W/m^2$ and $T_\infty = 295\ K$. The laser heat flux vector is assumed to be vertical with no horizontal component with a magnitude given by a Gaussian distribution, equation (12).

$$\frac{\partial \theta}{\partial n} = \frac{r_q}{k\Delta T_{m^\infty}}(\alpha \boldsymbol{q}_l \bullet \boldsymbol{n} - q_e - q_c) \tag{11}$$

$$q_l = \frac{3Q}{\pi r_q^2}\exp(3r^2) \tag{12}$$

The effect of the formation of the keyhole on the absorption of the laser energy was accounted for by assuming that the keyhole acts as a radiation cavity where the laser beam undergoes a large number of multiple reflections. With each reflection an additional amount of the laser energy is

absorbed. This effect is approximated using Equation (13) for the effective absorptivity of the key-hole, α.

$$\alpha = \alpha_0 + (1 - \alpha_0)(1 - F_{ko}) \tag{13}$$

F_{ko} is the radiation view factor from the keyhole internal surface to the opening of the keyhole and α_0 is the absorptivity of a flat molten metal surface. F_{ko} was approximated as the ratio of the area of the keyhole opening to that of the keyhole wall. Note that α varies from α_0, when no keyhole has formed (F_{ko}=1), to unity as the keyhole depth increases ($F_{ko} \rightarrow 0$).

The boundary conditions on the melt front for the energy equation are that the front has a temperature equal to the melting value and that the rate of movement of the front is determined by the difference between the energy fluxes into the front (i.e. from the molten phase) and out of the front (i.e. into the solid phase), as given by equation (14).

$$\boldsymbol{n} \bullet \nabla\theta_l - \boldsymbol{n} \bullet \nabla\theta_s = \frac{K_v}{S_b} \boldsymbol{n} \bullet \boldsymbol{v} \tag{14}$$

The Kirpichev number is, $K_v = Q/(r_a k \Delta T_m)$, the sub-cooling number is, $S_b = c_p \Delta T_m / H_{sf}$, and **v** is the velocity of the front. Constant temperature boundary conditions were applied on the side and bottom exterior surfaces of the solid phase.

Calculations were carried out for values for the laser power, Q, ranging from 1200 to 1800 W. A single laser pulse with a duration of 0.010 s was used along with a radius, r_q=0.5 mm, for the laser heat flux distribution. Properties for stainless steel were used in the calculations as given in Table 1.

The values of the parameters in the momentum equation for the conditions considered here are We^{-1}=120, Re^{-1}=0.01, and $\beta\Delta T_m/F_r$=0.02. This indicates that the pressure gradient is the dominant term, inertial forces are of secondary importance and viscous and buoyancy forces play only minor roles. The ratio We/Re is small (10^{-4}) so the force balance boundary condition on the free surface is dominated by surface tension, the recoil pressure and the pressure within the liquid. This implies that the pressure gradient, which is the dominant term in the momentum equation, is largely balanced by the recoil pressure and the effect of surface tension. The secondary role played by inertial forces means that the shape of the free surface may become quasi-static.

The inverse of the Peclet number has the value, Pe^{-1}=0.3, implying that heat transfer by the processes of convection and conduction have comparable magnitudes. The parameter in the melt front boundary condition, Kv/Sb=1, so the front velocity is expected to be sufficiently large to make the effect of the heat of fusion on the movement of the front significant.

The general purpose finite element fluid mechanics code, GOMA [13], was used for the calculations. A moving mesh technique was used where distinct portions of the mesh were made to track the time dependent shapes of the solid and liquid regions. The equations are solved using a full-Newton-coupled heat, mass, momentum, and mesh motion algorithm.

The moving mesh technique used in the calculations required an initial calculation using a fixed mesh that used a conduction formulation to obtain an initial (small) molten pool. This initial calculation starts from a condition where the material is completely solid and at a uniform temperature (θ=0) and proceeds until a small molten region is obtained. The shape of the molten pool in the fixed mesh calculation was defined by the melting temperature isotherm. This result was then used to start the moving mesh portion of the calculations by fitting the region of the moving mesh dedicated to the liquid region to the molten pool shape obtained from the fixed mesh. The initial condition for the moving mesh calculations also included the entire thermal field obtained from the fixed mesh calculation, which was mapped onto the moving mesh.

Figure 3 shows the initial form of the moving mesh and includes an enlargement of the liquid region which was obtained from the fixed mesh calculation. The mesh is composed of 9-node elements with 91 elements in the solid region and 74 elements in the liquid region and a total of 711 nodes in the mesh. The mesh spans a square domain measuring 1.5 mm on a side. The coordinate system is also shown in Figure 3.

Results

The weld pool shape and the thermal field for a laser power of 1800 W is shown at different times in Figure 4. At first the pool is small and shallow. Deformation of the free surface becomes significant early in the process and the shape of the liquid domain becomes that of a layer of uniform thickness that is spread over the melt front. As both the pool and keyhole depths increase with time the recoil pressure forces some of the liquid to flow outward and upward (see Figure 5) and the liquid rises above the top surface of the solid. The temperature distribution along the free surface becomes nearly uniform early in the process, except for the region near the outer perimeter. The temperature gradient near the perimeter of the free surface would result in a large thermocapillary force and associated fluid motion, but this effect is neglected in the current analysis. Note that near the center of the pool the free surface position (and propagation) closely follows that of the melt front. The displacement at the center of the free surface increases with time to a value of 0.48 mm at t=0.01s while the magnitude of the displacement rate increases with time from approximately 3 cm/s to a value of 8 cm/s at t=0.01s. This compares well with the scaling estimated in this paper for the melting rate, V_c=6.5 cm/s.

The predominant direction of the temperature gradient in the pool is everywhere perpendicular to the local orientation of the melt front. Thus, the small thickness of the molten region appears to make heat conduction the dominant mode of heat transfer in the pool. This large temperature gradi-

ent produces a large conduction heat transfer rate through the liquid resulting in rapid melting of the underlying solid. This rapid melting rate helps to confine the region ('heat affected zone') in the solid material that is heated to high temperature (i.e. T > 1050 K), which is not much larger than the pool itself as shown in Figure 4.

Figure 5 shows the velocity vectors in the weld pool. As material is melted and the pool thickens it is forced by a pressure gradient to flow upward along the melt front and some of the material rises above the top surface of the solid. The fluid velocities are on the order of 5 cm/s, which is approximately equal to the velocity of the front into the solid. This is also approximately equal to the value of the velocity scale discussed earlier for Q=1800W, V_c=6.5 cm/s.

Figure 6 shows in a semi-logarithm plot the laser power absorbed (i.e. integral of αq_l over the top surface) and the power lost by evaporation and by convection. Figure 7 shows the temperature at the center of the free surface and the effective absorptivity, α. The absorbed laser power increases with time due to the increase in α, which results from the increasing depth of the keyhole. The evaporation and convection losses increase due to the increasing size of the free surface at high temperature. The evaporation loss is much larger than the convection loss, but both losses which increase significantly with time are still much smaller than the absorbed laser power. The temperature of the free surface center increases rapidly from room temperature to approximately 3450K where it remains steady (approximately) thereafter. As seen from the results presented in Figure 5, the losses from the free surface are small, which is consistent with estimates by Kroos, et. al. [2]. The surface temperature is limited by heat conduction through the molten layer and into the underlying solid; that is, the molten layer thickness is sufficiently small that the absorbed laser power can be conducted through it with (moderate) surface temperatures that result in only small convection and evaporation losses.

The effect of power on weld shape is shown in Figure 8. On the left side of Figure 8 the results are shown at 0.01 s; and on the right side the results are shown at different times corresponding to the same net energy deposited in the material, ΔE_{net} = 4 J. The net deposited energy, ΔE_{net}, is obtained by integrating the absorbed laser power over time minus the convection and evaporation losses. Note that the results for Q = 1590 W are the same on the left and right sides, i.e. for Q = 1590 W, 4 J are deposited in 0.01 s. It is seen (on the left side) that the depth of the keyhole and weld pool both increase significantly with laser power for a given total heating time (0.01 s). The weld pool depth also increases with laser power for a given net deposited energy (ΔE_{net} = 4 J). Moreover, for a given net deposited energy of 4 J, the thickness of the zone heated to high temperatures (i.e. the 'heat affected zone') in the solid decreases with increasing laser power. These results show that the shapes and sizes of both the weld pool and 'heat affected zone' depend not only on the net deposited energy, but also on the laser power.

The efficiency of the laser welding process is given by $\Delta E_{net}/\Delta E_{tot}$, where ΔE_{tot} is the integral over time of the total laser power. The effect of power on the efficiency is shown in Figure 9. Also shown

is the net impulse imparted to the material by the vapor recoil force for a 0.01s laser pulse, obtained by integrating the vertical component (i.e. the z-component) of the recoil pressure over the free surface and over time. The results show that both the impulse and efficiency increase significantly with laser power. The efficiency and impulse are quantities that can be measured and used for model validation.

Summary

A model for the calculation of the mass, momentum and energy transport in a laser heated weld pool has been developed. The model uses a sub-model for the vapor recoil pressure on the free surface of the molten metal that results from rapid evaporation. This recoil pressure was shown to cause large deformations of the free surface such that the molten region becomes a thin layer between the free surface and melt front. As a result, the heat conduction through this thin layer is large and there is rapid melting of the underlying solid. The depth of penetration of the weld pool was shown to increase with laser power and total deposited energy. The size of the 'heat affected zone' in the solid phase adjacent to the weld pool was shown to decrease with increasing laser power for constant total energy deposited.

The conditions considered here for the magnitude of the laser heat flux were mild such that fluid velocities induced by the deformation of the free surface were small. Ejection of molten metal from the weld pool would not occur for these conditions due to the small fluid inertia. Extensions of this work considering conditions resulting in material ejection are needed because it is a source of welding defects.

A more complete evaporation model is needed that accounts for evaporation for free surface temperatures less than the (atmospheric) boiling temperature. Moreover, the assumption that the ambient air is semi-infinite in extent becomes invalid for deep keyholes because the shock wave will undergo reflections off the keyhole walls and generate a more complicated gas flow field than is assumed in this work. The results presented here have not yet been validated with comparisons to experimental data. However, the weld shape, efficiency and impulse imparted by the vapor recoil pressure were identified as quantities that are sensitive to the keyhole shape and are measureable, so they may be used for model validation in subsequent studies.

Acknowledgments

This work was supported by the United States Department of Energy under Contract DE-AC04-94AL85000. Sandia is a multiprogram laboratory operated by Sandia Corporation, a Lockheed Martin Company, for the U.S. Dept. of Energy.

Appendix

A velocity scale was derived in this paper that required an estimate for the heat conduction rate from

a melt front moving into a solid phase. This estimate was obtained assuming the heat conduction to be one-dimensional and the melt front to move with constant velocity, V_c, into a semi-infinite medium. Relative to the moving front the temperature distribution was assumed to be steady. This temperature distribution is governed by the equation (A1):

$$\rho c_p V_c \frac{d\theta}{dz} = k\frac{\partial^2 \theta}{\partial z^2} \tag{A1}$$

where $\theta=(T-T_\infty)/(T_m- T_\infty)$ is the non-dimensional temperature which varies from unity at the melt front (z=0) to zero at infinity. In equation (A1) V_c is considered to be the velocity of the medium relative to the front; that is, the medium is considered to be moving toward the front, $V_c<0$. The solution to this equation and boundary conditions is given by equation (A2) [14].

$$\theta = \exp(\rho c_p V_c z/k) \tag{A2}$$

From this result the heat conduction from the front into the solid phase can be obtained, as given by equation (A3).

$$k\frac{dT}{dz}\bigg|_{front} = (T_m - T_\infty)\rho c_p V_c \tag{A3}$$

The velocity scale can now be determined from a simplified form of the energy balance on the melt front, Equation (14), where the heat of fusion term is neglected; that is, the energy flux conducted into the front from the liquid phase, which is estimated to be that coming from the laser (approximated here as $\alpha_0 Q/r_q^2$), is equated with the heat flux conducted away from the front into the solid phase (estimated with equation A3). Solving for V_c gives the desired velocity scale, $V_c=\alpha_0 Q/(r_q^2 \rho c_p \Delta T_m)$. Note that retaining the heat of fusion term would give the result, $V_c=\alpha_0 Q/(r_q^2 \rho c_p \Delta T_m + r_q^2 \rho H_{sf})$. The second term in the denominator is smaller than the first for the conditions considered in this work, so it is neglected in order to simplify the result for the velocity scale.

Input Records:

None.

References

1. S.G. Lambrakos, E.A. Metzbower, J.H. Dunn, P.G. Moore, A numerical model of deep penetration laser welding, in: S.A. David and J.M. Vitek (Ed.s), Proceedings of the 3rd International Conference on Trends in Welding Research, ASM International, Materials Park, Ohio, 1992, pp. 51-55.

2. J. Kroos, U. Gratzke, G. Simon, Towards a self-consistent model of the keyhole in penetration laser beam welding, J. Phys. D: Appl. Phys. 26 (1993) 474-480.

3. R.K. Ganesh, W.W. Bowley, R.R. Bellantone, Y. Hahn, A model for laser hole drilling in metals, J. Computational Phys. 125 (1996) 161-176.

4. J. Dowden, P. Kapadia, A mathematical investigation of the penetration depth in keyhole welding with continuous CO_2 lasers, J. Phys. D: Appl. Phys, 28 (1995) 2252-2261.

5. P.S. Wei, C.Y. Ho, Beam focusing characteristics effect on energy reflection and absorption in a drilling or welding cavity of paraboloid of revolution, International Journal of Heat and Mass Transfer 41 (1998) 3299-3308.

6. P. Solana, J.L. Ocana, A mathematical model for penetration laser welding as a free-boundary problem, J. Phys. D: Appl. Phys. 30 (1997) 1300-1313.

7. A. Matsunawa, V. Semak, The simulation of front keyhole wall dynamics during laser welding, J. Phys. D: Appl. Phys. 30 (1997) 798-809.

8. S.C. Wang, P.S. Wei, Energy-beam redistribution and absorption in a drilling or welding cavity, Met. Trans. B 23B (1992) 505-511.

9. S.I. Anisimov, Vaporization of metal absorbin laser radiation, Soviet Physics JETP 27 (1) (1968) 182-183.

10. C. J. Knight, Theoretical modeling of rapid surface vaporization with back pressure, AIAA J. 17 (5) (1979) 519-523.

11. T. Iida and R.I.L. Guthrie, The physical properties of liquid metals*, Clarendon Press*, 1988, pp. 88.

12. G.K. Batchelor, An introduction to fluid dynamics, Cambridge University Press, 1967. pp. 60-64.

13. P.R. Schunk, P.A. Sackinger, R.R. Rao, K.S. Chen, R.A. Cairncross, T.A. Baer, D.A. Labreche, GOMA 2.0 – A full-newton finite element program for free and moving boundary problems with coupled fluid/solid momentrum, energy, mass and chemical species transport: User's Guide, Sandia Report, SAND97-2404, Sandia National Laboratories, Albuquerque, NM, September 1998.

14. H.S. Carslaw, J.C. Jaeger, Conduction of heat in solids, Oxford, 1959, pp. 291-293.

Table 1. Thermal physical properties of stainless steel (304)

Property	Value
Specific heat, c_p – J/(Kg K)	669
Thermal conductivity, k – W/(m K)	45
Density, ρ - Kg/m^3	7000
Viscosity, μ - Kg/(m s)	0.00225
Thermal expansion coefficient, β - 1/K	10^{-5}
Surface tension, σ - N/m	1.76
Absorptivity, α_0	0.2
Latent heat of evaporation, H_{fg} – J/Kg	$6.3 \cdot 10^6$
Latent heat of fusion, H_{sf} – J/Kg	$3 \cdot 10^5$
Boiling temperature , T_b - K	3375
Melting temperature, T_m - K	1808

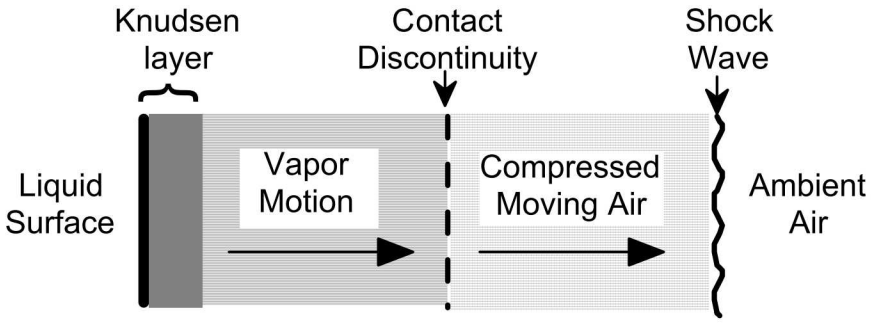

Figure 1. A schematic of the one-dimensional gas dynamic flow of vapor and air away from a liquid surface at elevated temperature where the evaporation rate is steady.

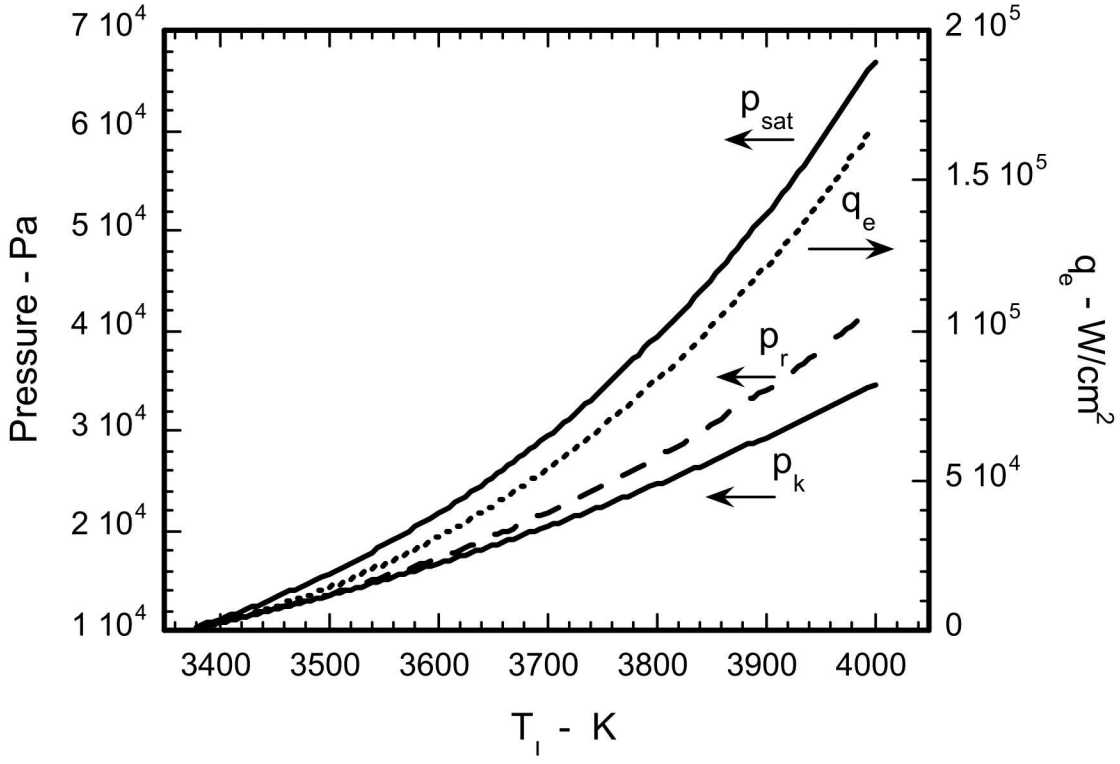

Figure 2. The saturation pressure, recoil pressure, static pressure at the outer edge of the Knudsen layer, and the rate of energy loss by evaporation versus liquid surface temperature.

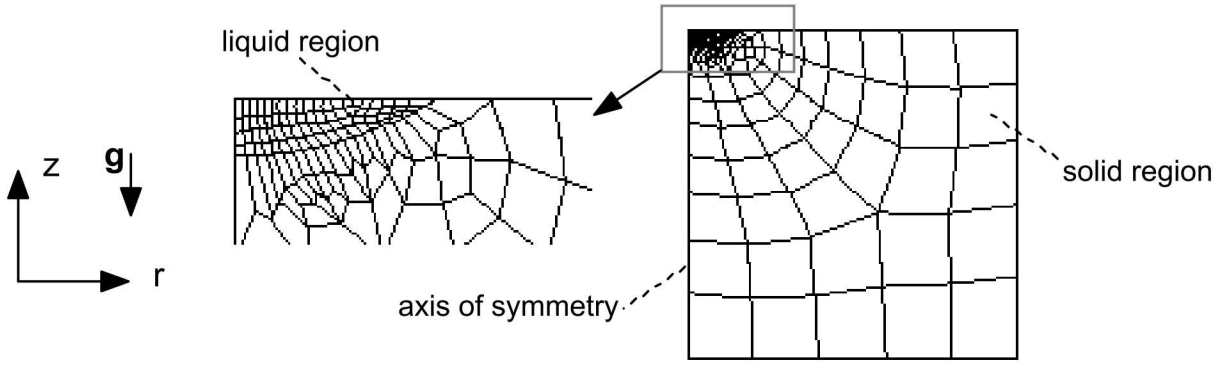

Figure 3. The finite element mesh used in the calculations.

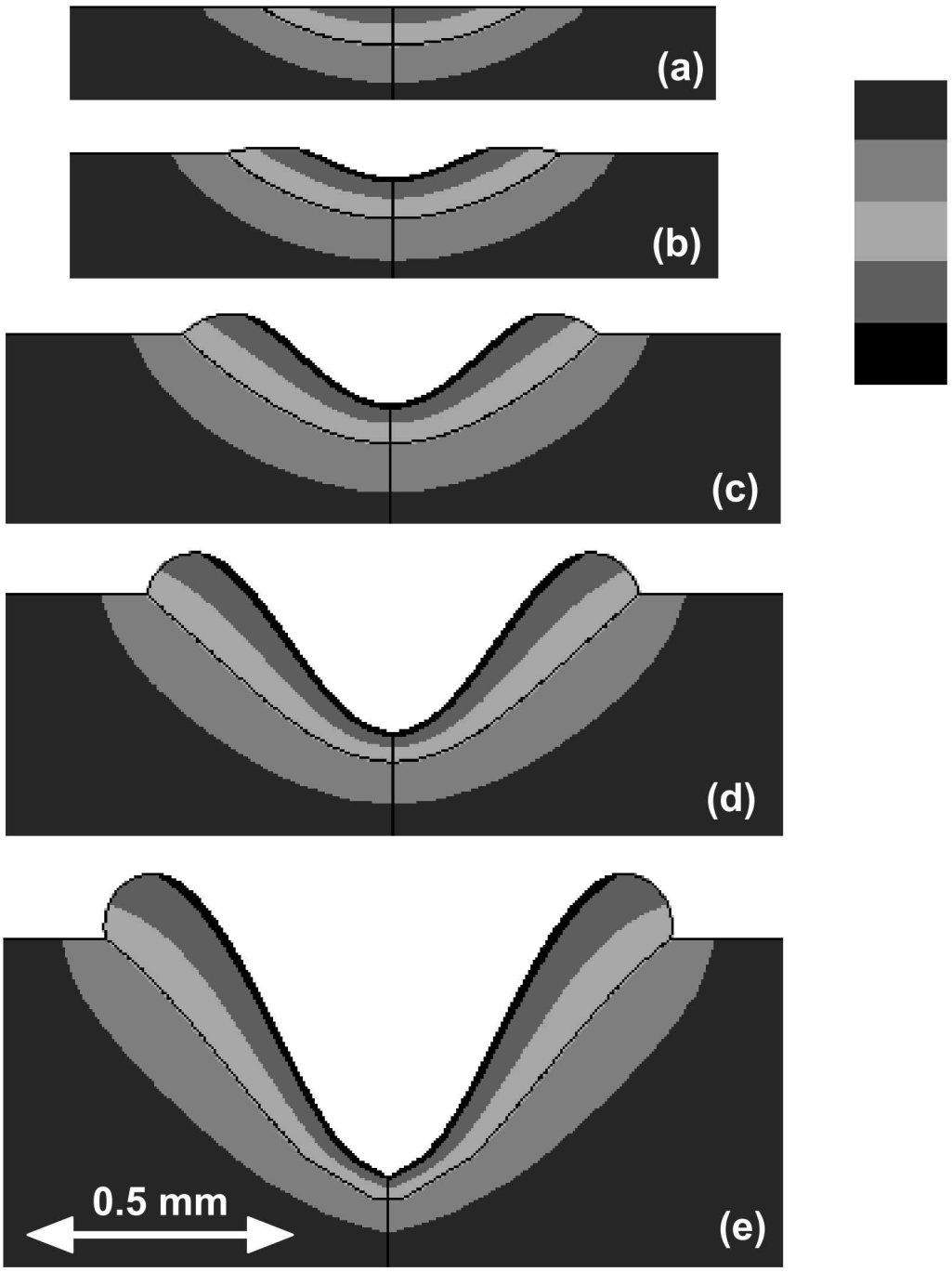

Figure 4. The temporal development of the weld pool shape and temperature field for Q=1800 W. t = 0.001s (a), 0.0025s (b), 0.005s (c), 0.0075s (d), 0.01s (e)

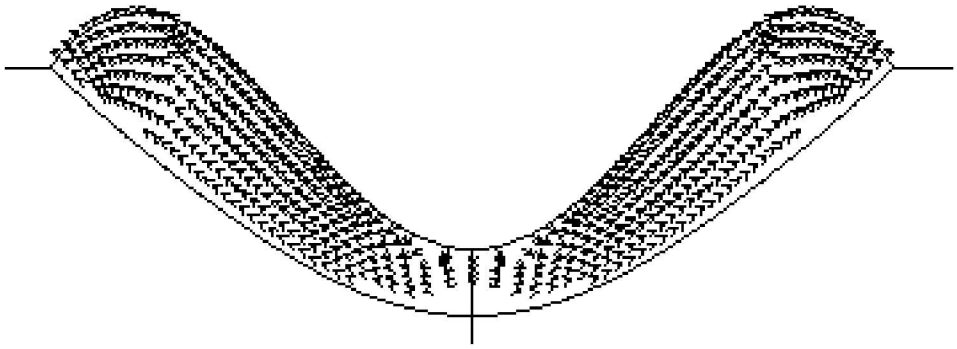

Figure 5. The velocity vectors in the weld pool at t = 0.006 s for Q = 1800 W.

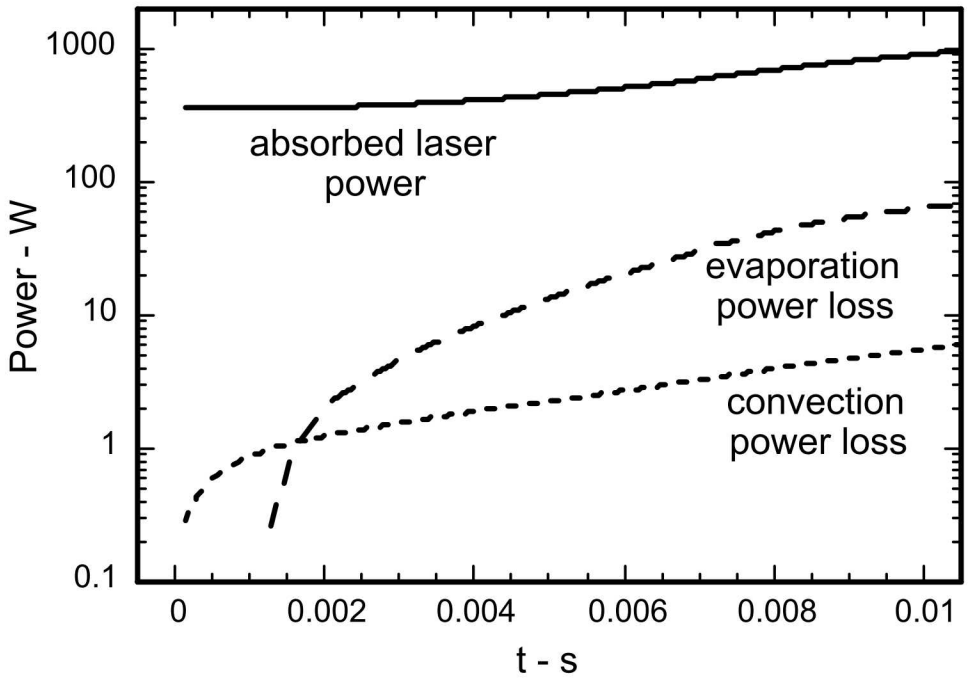

Figure 6. The absorbed laser power, and rates of energy loss by evaporation and convection, for Q = 1800W.

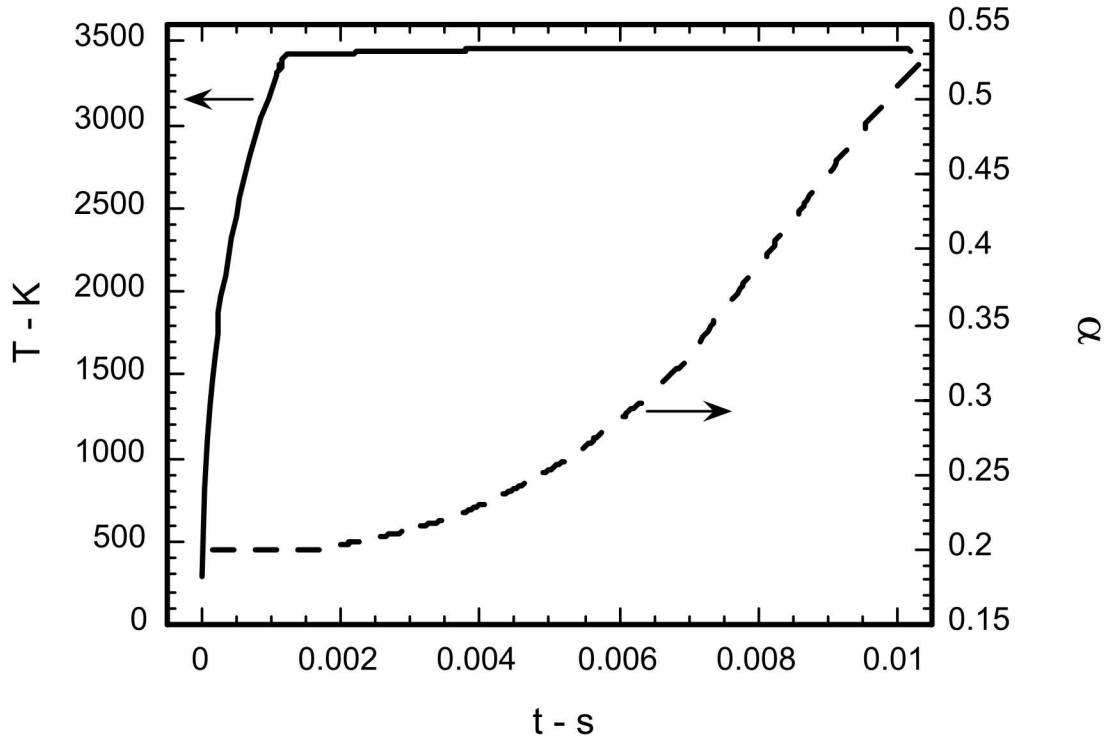

Figure 7. The temperature at the center of the free surface and the effective absorptivity of the laser energy by the keyhole as a function of time. Laser power = 1800W.

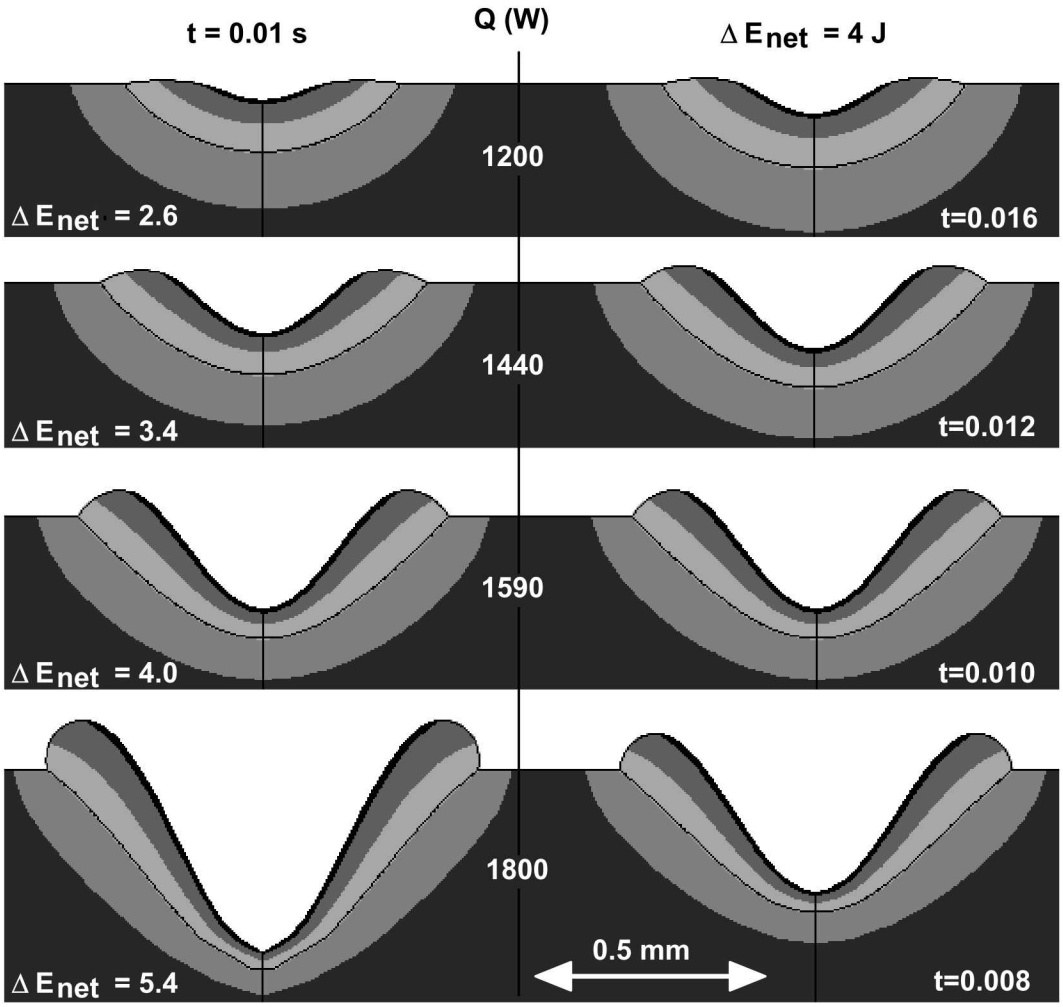

Figure 8. The effect of power on weld pool shape. On the left side of the figure the results are at the same time of 0.01s, and on the right side the results are at the same net deposited energy of 4 J. The same temperature scale used in Figure 4 is used here.

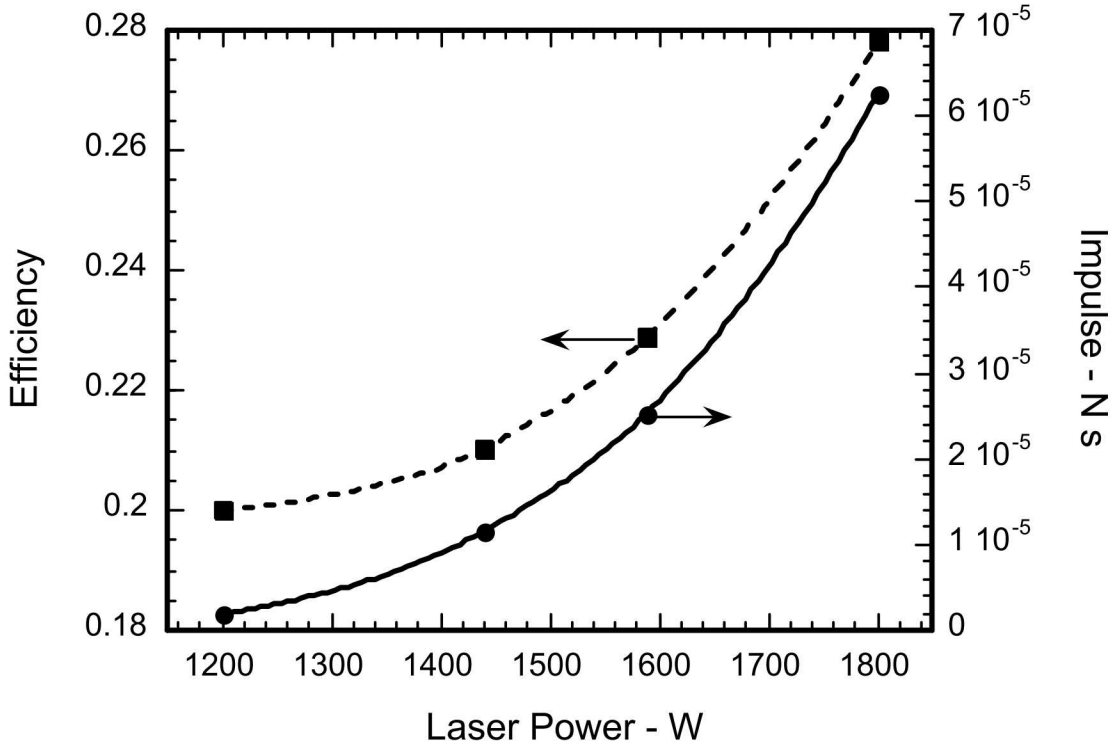

Figure 9. The efficiency of the laser spot welding process (fraction of laser energy absorbed by the metal) and the total impulse imparted to the metal by the vapor recoil pressure for a 0.01 s pulse, as a function of laser power.